

# Taming the Chlorine Radical: Enforcing Steric Control over Chlorine Radical-Mediated C–H Activation

Miguel I. Gonzalez,<sup>†</sup> David Gygi,<sup>†</sup> Yangzhong Qin,<sup>†</sup> Qilei Zhu,<sup>†</sup> Elizabeth J. Johnson,<sup>†</sup> Yu-Sheng Chen,<sup>‡</sup> Daniel G. Nocera<sup>\*,†</sup>

<sup>†</sup>Department of Chemistry and Chemical Biology, Harvard University, 12 Oxford Street, Cambridge, MA 02138, United States

<sup>‡</sup>ChemMatCARS, The University of Chicago, Argonne, IL 60439, United States

**ABSTRACT:** Chlorine radicals readily activate C–H bonds, but the high reactivity of these intermediates precludes their use in regioselective C–H functionalization reactions. We demonstrate that the secondary coordination sphere of a metal complex can confine photoeliminated chlorine radicals and afford steric control over their reactivity. Specifically, a series of iron(III) chloride pyridinediimine complexes exhibit activity for photochemical C(sp<sup>3</sup>)–H chlorination and bromination with selectivity for primary and secondary C–H bonds, overriding thermodynamic preference for weaker tertiary C–H bonds. Transient absorption spectroscopy reveals that Cl• remains confined through formation of a Cl•|arene complex with aromatic groups on the pyridinediimine ligand. Furthermore, photocrystallography confirms that this selectivity arises from the generation of Cl• within the steric environment defined by the iron secondary coordination sphere.

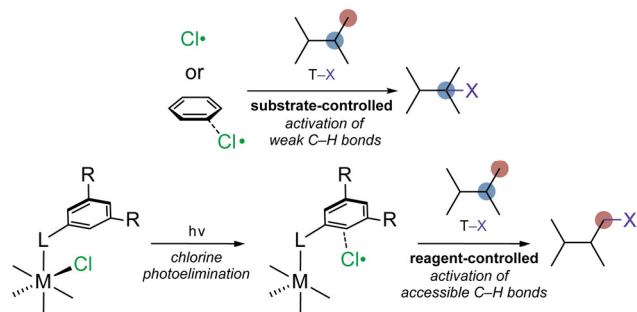
## INTRODUCTION

Direct functionalization of C–H bonds embodies the cleavage of the most prevalent, yet one of the most unreactive linkages in organic molecules.<sup>1–5</sup> To overcome the challenge that the reticent C–H bond presents, research has focused on strategies to generate and control high-energy intermediates that are sufficiently reactive to activate C–H bonds.<sup>6–12</sup> In particular, chlorine radicals have been employed as powerful hydrogen-atom abstraction reagents for nearly a century<sup>5,13,14</sup> and more recently, in the rapidly growing field of photoredox catalysis.<sup>12,16</sup> Photogenerated chlorine radicals have been identified as key intermediates in photoredox methods for the alkylation,<sup>17–20</sup> alkenylation,<sup>21</sup> arylation,<sup>22–24</sup> acylation,<sup>22,25</sup> and amination<sup>26,27</sup> of C(sp<sup>3</sup>)–H bonds. However, catalyst-controlled selectivity in chlorine radical-mediated C–H activation reactions has remained a significant challenge that has not yet been achieved.<sup>12,15</sup>

Driven by the thermodynamically favorable formation of the H–Cl bond (BDE = 103 kcal/mol), chlorine radicals readily cleave aliphatic C–H bonds, including the strong C–H bonds of primary carbons (BDE = 101.1 kcal/mol for ethane) and of methane (BDE = 105.0 kcal/mol).<sup>5</sup> This inherently high reactivity, however, leads to nearly indiscriminate activation of substrates with different C–H bonds. Indeed, the selectivities of chlorine radicals in hydrogen atom transfer reactions show low sensitivity to relative C–H bond strengths, favoring substrate-controlled activation of weaker 3° C–H bonds over 1° and 2° C–H bonds (Scheme 1).<sup>14</sup> As a consequence, chlorine-radical mediated C–H functionalization reactions often require careful selection of feedstocks or energy-intensive separation of complex product mixtures.<sup>5</sup>

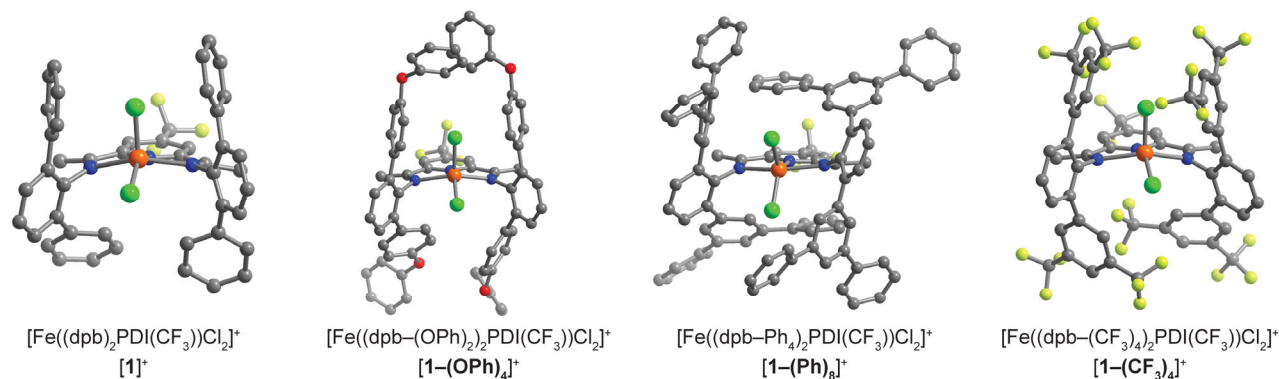
Unlike metal complexes and organic reagents developed for selective C–H functionalization reactions<sup>28–37</sup> chlorine radicals lack direct structural handles to tune their reactivity. In the presence of aromatic solvents, however, these radicals can form Cl•|arene charge-transfer complexes. These complexes exhibit increased selectivity toward the weakest C–H bonds in radical chlorination reactions

**Scheme 1.** Proposed strategy for selective C–H activation using photoeliminated chlorine radicals.



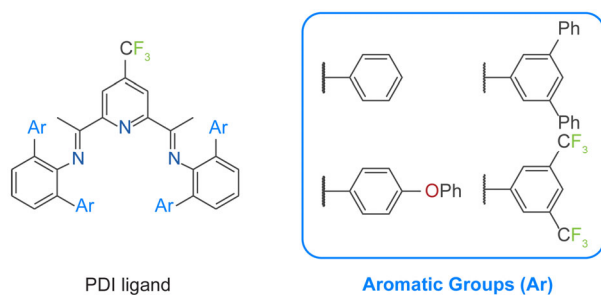
(Scheme 1) due to electronic stabilization of Cl• by the aromatic ring (~3 kcal/mol for Cl•|benzene with respect to Cl• in solution).<sup>22,38,39</sup> In general, electron donating substituents on the arene of these complexes improve site selectivity for the weakest C–H bond, while electron withdrawing groups decrease selectivity.<sup>39</sup>

Cl•|arene adducts can also form upon association of photoeliminated chlorine radicals with aromatic substituents in the secondary coordination sphere of a metal chloride complex.<sup>40–42</sup> In these systems, excitation of the ligand-to-metal charge-transfer (LMCT) bands of the metal complex results in cleavage of an M–Cl bond with concomitant reduction of the metal center and dissociation of Cl•, which can then associate to an aromatic group on the ligand to form a Cl•|arene adduct. We recently investigated the trajectory of a chlorine radical eliminated from an iron(III) pyridinediimine (PDI) complex and unveiled that the formation of a Cl•|arene adduct guides the radical toward activating specific C–H bonds in the solid state.<sup>42</sup> Building upon this work, we envisioned that arene–Cl• interactions could be leveraged to confine a photoeliminated chlorine radical within the secondary coordination sphere of a metal complex, thereby affording structural control over its reactivity (Scheme



**Figure 1.** Solid-state structures of  $[1][FeCl_4]$ ,  $[1-(OPh)_4][FeCl_4]$ ,  $[1-Ph_8][B(C_6F_5)_4]$ , and  $[1-(CF_3)_8][FeCl_4]$  as determined by single-crystal X-ray diffraction at 15 K. Orange, green, light green, red, blue, gray spheres represent Fe, Cl, F, O, N, C atoms, respectively. Counteranions, solvent molecules, and hydrogen atoms are omitted for clarity.

**Scheme 2.** Chemical structures of the PDI ligands.



1). To this end, we synthesized a series of iron(III) PDI complexes featuring aromatic groups that define a steric environment for photoeliminated chlorine radicals. As a result, we show here that these complexes enforce steric selectivity for more accessible C–H bonds over weaker C–H bonds in chlorine-radical mediated C–H functionalization reactions.

## RESULTS AND DISCUSSION

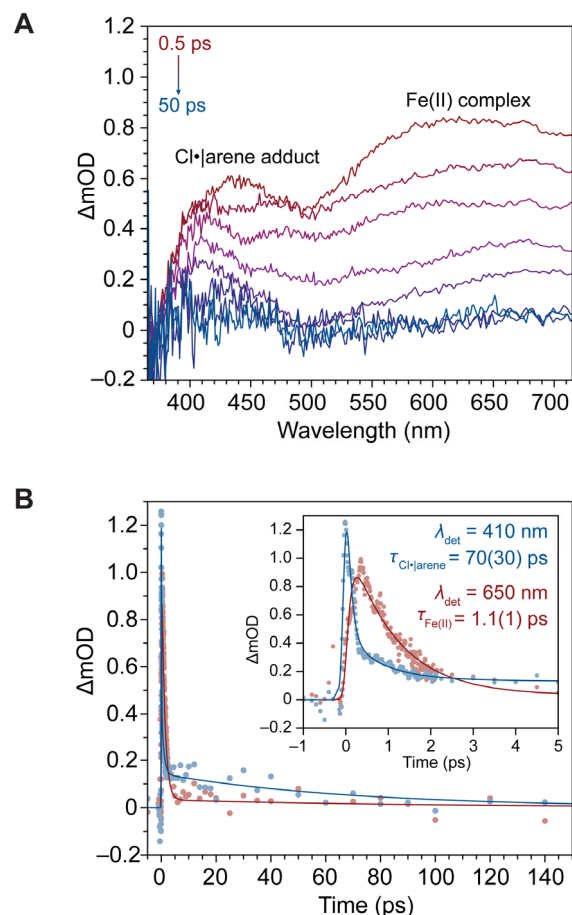
### Synthesis and Characterization of Iron(III) PDI Complexes.

Recognizing that PDI ligands situate N-aryl *ortho* substituents near the axial sites of their corresponding metal complexes,<sup>43</sup> we designed the PDI ligand (dpb)<sub>2</sub>PDI(CF<sub>3</sub>) (Scheme 2) to form an iron(III) chloride complex with phenyl substituents proximate to its apical Fe–Cl bond, from which Cl• elimination occurs.<sup>42</sup> Reaction of this ligand with two equivalents of FeCl<sub>3</sub> in dichloromethane at 25 °C yields the  $[FeCl_4]^-$  salt of the cationic complex  $[Fe((dpb)_2PDI(CF_3)Cl_2)]^+$  ( $[1]^+$ ), which was isolated as a dark red crystalline solid. Characterization of  $[1][FeCl_4]$  by single-crystal X-ray diffraction reveals that the PDI complex adopts a distorted square-pyramidal geometry with two chloride ligands occupying the apical and basal sites of the iron center (Figure 1). Two phenyl substituents surround the apical chloride ligand, creating a pocket in which photoeliminated chlorine radicals can reside. To tune the steric and electronic environment of this pocket, additional analogues of  $[1]^+$  (Figure 1 and Figure S1) were prepared using PDI ligands bearing –OPh, –Ph, and –CF<sub>3</sub> substituents on their aromatic rings (Scheme 2). The PhO- and CF<sub>3</sub>-functionalized analogues ( $[1-(OPh)_4]^+$  and  $[1-(CF_3)_8]^+$ ) feature structures similar to  $[1]^+$ , whereas the Ph-functionalized complex ( $[1-Ph_8]^+$ ) exhibits a trigonal-bipyramidal geometry with two equatorial chloride ligands. Only one aromatic ring was located next to each of the chloride

ligands in  $[1-Ph_8]^+$ , which suggests that the steric bulk of the phenyl substituents prevents two rings from approaching the same face of the complex.

**Time-Resolved Photochemistry.** Solution-phase transient absorption (TA) spectroscopy experiments were performed to probe for the formation of the Cl•|arene adduct. Because  $[FeCl_4]^-$  can photoeliminate Cl• under the laser wavelength of the TA experiment ( $\lambda_{exc} = 360$  nm), the counteranion of  $[1][FeCl_4]$  was replaced with  $[B(C_6F_5)_4]^-$ . Femtosecond-resolved TA measurements on a solution of  $[1][B(C_6F_5)_4]$  in nitromethane show the prompt formation of two broad signals with maxima at ~435 nm and ~620 nm after laser excitation (Figure 2A). Based on previous work following the formation of a similar adduct after Cl• elimination from a cationic iron(III) PDI complex,<sup>42</sup> we assign the peak at ~435 nm to arise predominantly from the Cl•|arene adduct and the peak at ~620 nm to the iron(II) complex formed after Fe–Cl bond cleavage (Figure S12). Single-wavelength kinetics measurements monitored at 410 and 650 nm reveal that the two processes contribute to the decay of both signals (Figure 2B). The first process is consistent with the rapid recombination of iron(II) with Cl• that does not form an adduct ( $\tau_{Fe(II)} = 1.1(1)$  ps;  $\lambda_{det} = 650$  nm), while the slower process is ascribed to decay of the Cl•|arene adduct ( $\tau_{Cl\cdot|arene} = 70(30)$  ps;  $\lambda_{det} = 410$  nm). Both signals eventually decay to zero, indicating that the two processes result in regeneration of the initial iron(III) PDI complex. These experiments reveal that the photoeliminated chlorine radical either undergoes rapid back reaction with iron(II) or associates with the secondary coordination sphere to form a Cl•|arene adduct, which is then poised to react with substrate molecules proximate to the complex.

**Photohalogenation Experiments.** Metal chloride complexes that undergo chlorine photoelimination have been exploited as reagents in C–H functionalization reactions.<sup>15–18,21,22,24–27,44–51</sup> In general, these reactions remain governed by the thermodynamic preference of chlorine radicals for weaker C–H bonds, which leads to site selectivities that follow the trend 3° > 2° > 1°.<sup>14</sup> We anticipated that steric hindrance around the photoeliminated chlorine radical would favor activation of more accessible 1° and 2° C–H bonds.<sup>32,35</sup> Conversely, the absence of a steric environment would manifest as increased selectivity for 3° C–H bonds due to stabilization of the radical by arene–Cl• interactions.<sup>38,39</sup> Thus, the iron(III) PDI complexes were evaluated in the photochlorination of 3-methylpentane (**2**)—a substrate with 1°, 2°, and 3° C–H bonds—to probe for selective C–H activation by photoeliminated chlorine radicals. Photochlorination reactions were conducted using 440 nm light in nitromethane with

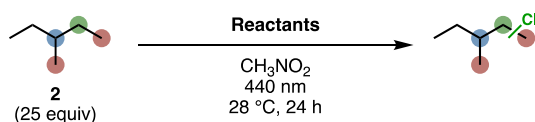


**Figure 2.** (A) Evolution of the TA spectra of a solution of  $[1][B(C_6F_5)_4]$  in nitromethane (red to blue lines) after excitation with a 360 nm laser pulse. (B) Single-wavelength kinetics traces monitored at 410 nm (light blue circles) and 650 nm (light red circles) fit (blue and red lines, respectively) with a biexponential lifetimes.

an excess of substrate (25 equiv) to avoid formation of dihalogenated products. Reactions using  $[1][FeCl_4]$ ,  $[1-(OPh)_4][FeCl_4]$ ,  $[1-Ph_3][FeCl_4]$ , and  $[1-(CF_3)_3][FeCl_4]$  yielded monochlorinated products (Entry 1, Table 1 and Table S3) as determined by gas chromatography (GC). No chlorinated products were observed in a control reaction conducted in the absence of light (Entry 4, Table 1), confirming that C–H activation occurs photochemically. The PDI complexes exhibit higher 2°/3° and 1°/3° selectivity as compared to  $FeCl_3$  and  $[(Ph_3P)_2N][FeCl_4]$  (Entries 2 and 3, Table 1), which give product distributions close to that of free chlorine radicals. These results suggest that the iron(III) PDI complexes generate chlorine radicals within an environment that confers steric selectivity for less hindered 1° and 2° C–H bonds. Expecting that the addition of benzene would liberate  $Cl\cdot$  from the PDI complex through competitive formation of  $Cl\cdot$ -benzene adducts, we performed a photochlorination reaction using  $[1][FeCl_4]$  in a 1:1 (v/v) solution of benzene and nitromethane (Entry 5, Table 1). The presence of benzene shifts selectivity towards 3° C–H functionalization, corroborating the role of arene- $Cl\cdot$  interactions in confining chlorine radicals within the secondary coordination sphere. These results also suggest that C–H activation is not mediated by the iron center or other radical intermediates, as these species should exhibit similar selectivity in the presence of exogenous benzene.

The formation of each chlorinated product molecule requires two chlorine-atom equivalents, one to abstract a hydrogen atom from the substrate and another to add onto the resulting carbon-centered radical.<sup>52</sup> Thus, we expected one mole of  $[Fe(PDI)Cl_2][FeCl_4]$  to afford one equivalent of chlorinated product along with the reduction of two iron(III) centers to iron(II), assuming that the cationic iron(III) PDI complex generates one chlorine atom equivalent, while the  $[FeCl_4]^-$  counteranion provides the second equivalent. To determine the origin of the excess product, photochlorination reactions were conducted in different solvents using  $FeCl_2$  as a reagent (Table S13). Chlorinated products were observed in the reaction

**Table 1.** Photochlorination of 3-methylpentane using  $[1][FeCl_4]$ ,  $[1][B(C_6F_5)_4]$ ,  $FeCl_3$ , and  $[(Ph_3P)_2N][FeCl_4]$ .



Entry	Reactants	Normalized 1° : 2° : 3° product ratio <sup>a</sup>	Turnover <sup>b</sup>
1	$[1][FeCl_4]$	24.5(5) : 50(2) : 25(2)	1.41(1)
2	$FeCl_3$	17.8(5) : 35(1) : 47(2)	1.40(7)
3	$[(Ph_3P)_2N][FeCl_4]$	11.9(1) : 35.8(1) : 52.36(5)	1.68(5)
4	$[1][FeCl_4]$ (no light)	—	0
5	$[1][FeCl_4]$ , $C_6H_6$ (280 equiv)	8 : 33 : 59	1.8
6	$[1][B(C_6F_5)_4]$	16 : 42 : 42	0.25
7	$[1][B(C_6F_5)_4]$ , $CCl_4$ (550 equiv)	34.7(3) : 63.7(3) : 1.6(6)	0.7(1)
8	$(dpb)_2PDI(CF_3)$ , $CCl_4$ (550 equiv)	8 : 25 : 67	0.35

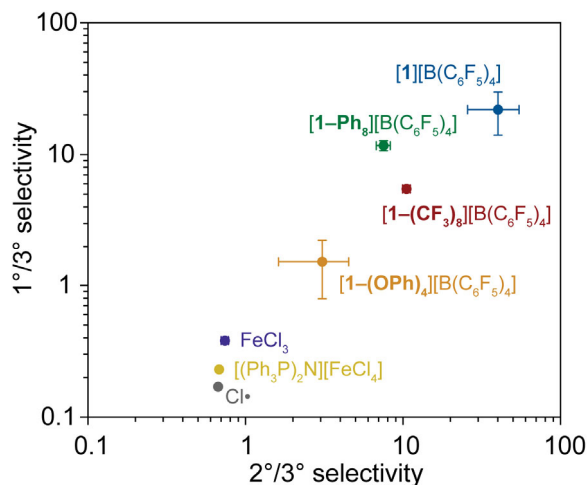
All product ratios and turnover numbers were determined by GC analysis. <sup>a</sup> All product ratios are normalized with respect to the number of 1°, 2°, and 3° C–H bonds. <sup>b</sup> For reactions with  $CCl_4$ , turnovers are reported as moles product per mole  $Fe(III)$  (Entry 7) or mole PDI ligand (Entry 8). For reactions without an external functional group donor, turnovers are reported as moles product per two moles of  $Fe(III)$ . Values obtained as an average of three replicates are reported with the standard deviation enclosed in parenthesis.



performed in nitromethane, while only trace amounts were obtained from reactions conducted in either  $\alpha,\alpha,\alpha$ -trifluorotoluene or acetonitrile. These results suggest that the additional chlorinated products stem from regeneration of iron(III) chloride species through reoxidation of iron(II) in the presence of nitromethane and not chlorine photoelimination from iron(II) chloride species, which should occur in other solvents. Comparison of the reduction potentials of the iron(III) complexes ( $E^\circ_{\text{Fe(III)/Fe(II)}} = 0.2\text{--}0.47\text{ V}$  vs  $\text{Fc}/\text{Fc}^+$ ;  $\text{Fc}$  = ferrocene; Figure S14) with that of nitromethane ( $E^\circ = -1.3\text{ V}$  vs  $\text{Fc}/\text{Fc}^+$ )<sup>53</sup> indicates that oxidation of iron(II) intermediates by nitromethane is thermodynamically uphill by  $\sim 1.5\text{--}1.8\text{ V}$ . To demonstrate that this oxidation can occur photochemically, a mixture of  $\text{FeCl}_2$  and  $(\text{dpb})_2\text{PDI}(\text{CF}_3)$  was photolyzed in nitromethane using 440 nm light. Monitoring the reaction by UV-vis spectroscopy (Figure S13) confirmed the formation of the iron(III) complex  $[\text{Fe}((\text{dpb})_2\text{PDI}(\text{CF}_3)\text{Cl}_2)]^+$ , which was also detected by high-resolution mass spectrometry (Figure S16). Moreover, photochlorination of 3-methylpentane using a mixture of  $\text{FeCl}_2$  and  $(\text{dpb})_2\text{PDI}(\text{CF}_3)$  in the presence of  $\text{CCl}_4$  also shows selectivity for  $2^\circ$  and  $1^\circ$  chlorinated products (Table S13). Together, these experiments demonstrate that photochemical oxidation of iron(II) intermediates by nitromethane regenerates the iron(III) PDI complex, leading to catalytic turnover of the photochlorination reaction.

The photochlorination activity of  $[(\text{Ph}_3\text{P})_2\text{N}][\text{FeCl}_4]$  indicates that the  $[\text{FeCl}_4]^-$  counteranion can undergo undesired chlorine radical elimination and lower the overall photochlorination selectivity. Comparison of the UV-vis absorption spectra of  $[(\text{Ph}_3\text{P})_2\text{N}][\text{FeCl}_4]$  with the spectra of the  $[\text{FeCl}_4]^-$  and  $[\text{B}(\text{C}_6\text{F}_5)_4]^-$  salts of the iron(III) PDI complexes (Figures S11) show that  $[\text{FeCl}_4]^-$  absorbs much less light in the emission spectrum of the 440 nm lamp used in the photochlorination reactions. To further interrogate the influence of irradiation wavelength on photochlorination,  $[\mathbf{1}][\text{FeCl}_4]$  was evaluated in reactions using 390, 456, and 467 nm LED lamps (Table S14). The reaction performed under 390 nm lamp resulted in poorer selectivity but higher yields, which is in line with the greater absorbance of both  $[\mathbf{1}]^+$  and  $[\text{FeCl}_4]^-$  at this wavelength. Conversely, reactions using wavelengths longer than 440 nm gave higher selectivities but lower yields due to weaker absorption by  $[\mathbf{1}]^+$ . These observations reveal that the  $[\text{FeCl}_4]^-$  salts of the iron(III) PDI complexes maintain photochlorination selectivity when irradiated with  $\geq 440\text{ nm}$  light due to stronger absorption by the PDI complexes at these wavelengths compared to  $[\text{FeCl}_4]^-$ .

To circumvent the generation of free  $\text{Cl}\cdot$  from  $[\text{FeCl}_4]^-$  and improve C–H activation selectivity, photochlorination reactions were performed using the  $[\text{B}(\text{C}_6\text{F}_5)_4]^-$  salts of the iron(III) PDI complexes ( $[\text{Fe}(\text{PDI})\text{Cl}_2][\text{B}(\text{C}_6\text{F}_5)_4]$ ). Under the same reaction conditions employed for  $[\mathbf{1}][\text{FeCl}_4]$ ,  $[\mathbf{1}][\text{B}(\text{C}_6\text{F}_5)_4]$  showed low activity and selectivity (Entry 6, Table 1), suggesting that  $[\mathbf{1}]^+$  cannot efficiently chlorinate the substrate radicals formed after C–H activation. Anticipating that the carbon-centered radicals combine to form C–C coupled products in the absence of a functional group donor, we analyzed the products for the functionalization of toluene using either  $[\mathbf{1}][\text{B}(\text{C}_6\text{F}_5)_4]$  or  $\text{FeCl}_3$  under the same conditions (Table S4). The reaction with  $[\mathbf{1}][\text{B}(\text{C}_6\text{F}_5)_4]$  gave rise to both the homocoupled product, bibenzyl, and the chlorinated product, benzyl chloride, with a product ratio of 53:47 bibenzyl to benzyl chloride. In contrast, photolysis of toluene with  $\text{FeCl}_3$  predominantly yielded benzyl chloride. These results revealed that an external Cl-atom donor was necessary to trap carbon-centered radicals formed after C–H activation by  $\text{Cl}\cdot$  eliminated from the  $[\text{Fe}(\text{PDI})\text{Cl}_2][\text{B}(\text{C}_6\text{F}_5)_4]$  complexes.



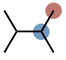
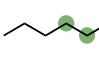
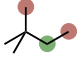
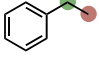

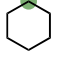

**Figure 3.** Comparison of  $1^\circ/2^\circ$  and  $2^\circ/3^\circ$  C–H chlorination selectivities of  $[\mathbf{1}][\text{B}(\text{C}_6\text{F}_5)_4]$  (blue),  $[\mathbf{1}-(\text{OPh})_4][\text{B}(\text{C}_6\text{F}_5)_4]$  (orange),  $[\mathbf{1}-\text{Ph}_8][\text{B}(\text{C}_6\text{F}_5)_4]$  (green),  $[\mathbf{1}-(\text{CF}_3)_4][\text{B}(\text{C}_6\text{F}_5)_4]$  (red),  $[(\text{Ph}_3\text{P})_2\text{N}][\text{FeCl}_4]$  (yellow),  $\text{FeCl}_3$  (violet), and  $\text{Cl}\cdot$  (gray). With the exception of  $\text{Cl}\cdot$ , all selectivities were determined from the photochlorination of 3-methylpentane. Error bars correspond to the standard deviation obtained for three replicates.

Accordingly, addition of the Cl-atom donor  $\text{CCl}_4$  (550 equiv), which forms trichloromethyl radicals ( $\text{Cl}_3\text{C}\text{--H}$  BDE = 93.8(6) kcal/mol<sup>54</sup>) too weak to activate strong C–H bonds, enabled  $[\mathbf{1}][\text{B}(\text{C}_6\text{F}_5)_4]$  to perform the highly selective C–H photochlorination (Entry 7, Table 1 and Table S5).

We note that selectivity decreases as the reaction approaches and exceeds one turnover (Figure S15), as a result of the loss of PDI ligand from the complex over the course of the reaction. This result also suggests that unselective photochlorination in the absence of  $\text{CCl}_4$  (Entry 6, Table 1) arises from formation of free  $\text{FeCl}_3$ , which can both eliminate  $\text{Cl}\cdot$  and chlorinate carbon-centered radicals. Recognizing that photolysis of  $\text{CCl}_4$  can also generate  $\text{Cl}\cdot$ , we performed a control photochlorination experiment with  $\text{CCl}_4$  and unmetalated  $(\text{dpb})_2\text{PDI}(\text{CF}_3)$  (Entry 8, Table 1). These conditions favored chlorination of  $3^\circ$  C–H bonds, showing that radical species derived from photolysis of  $\text{CCl}_4$  cannot account for the observed steric selectivity.

Photochlorination reactions using the  $[\text{Fe}(\text{PDI})\text{Cl}_2][\text{B}(\text{C}_6\text{F}_5)_4]$  salts demonstrate enhancement of the C–H activation selectivity of  $\text{Cl}\cdot$  by factors of 130 for  $1^\circ/3^\circ$  and by 60 for  $2^\circ/3^\circ$  (Figure 3 and Table S5). Moreover, when normalized to the number of C–H bonds,  $[\mathbf{1}][\text{B}(\text{C}_6\text{F}_5)_4]$  shows higher  $1^\circ/3^\circ$  and  $2^\circ/3^\circ$  site selectivities of 22(8) and 40(14), respectively, as compared to that of a previously reported amidyl radical<sup>35</sup> (3.5 and 2.2, respectively) though slightly smaller  $1^\circ/2^\circ$  site selectivities (1.6 for amidyl radicals vs 0.55 for  $[\mathbf{1}][\text{B}(\text{C}_6\text{F}_5)_4]$ ). The overall selectivity of these compounds follows the trend  $2^\circ > 1^\circ > 3^\circ$ , which arises from a combination of the steric selectivity against  $3^\circ$  C–H bonds afforded by the PDI complexes and the inherent preference of  $\text{Cl}\cdot$  for weaker C–H bonds. The relative selectivities of these complexes depend on the substituents on their aromatic rings, further supporting that selective C–H activation proceeds through a  $\text{Cl}\cdot$ -arene intermediate. Of the four complexes, the PhO-functionalized compound,  $[\mathbf{1}-(\text{OPh})_2][\text{B}(\text{C}_6\text{F}_5)_4]$ , shows the least pronounced steric selectivity, which is consistent with increased electronic stabilization of photoeliminated  $\text{Cl}\cdot$  by the electron-rich rings on the ligand.<sup>39</sup> The complex  $[\mathbf{1}-\text{Ph}_8][\text{B}(\text{C}_6\text{F}_5)_4]$  also exhibits lower selectivity against  $3^\circ$  C–H bonds compared to  $[\mathbf{1}][\text{B}(\text{C}_6\text{F}_5)_4]$ , which is attributed to the complex having only one

**Table 2.** Substrate scope for photochlorination using  $[\mathbf{1}][\text{B}(\text{C}_6\text{F}_5)_4]$  and  $\text{FeCl}_3$ .

Reactants							
	3	4	5	6	7	8	9
$[\mathbf{1}][\text{B}(\text{C}_6\text{F}_5)_4]$	96.9(4) : 3.1(4)	40.3(6) : 59.7(6)	44(9) : 56(9)	91(8) : 9(8)	25(2) : 75(2)	0.8(1)	24(2) : 76(2)
$\text{CCl}_4$ (550 equiv)	0.19(6)	0.31(7)	0.29(5)	0.10(4)	4.5(5)		2.5(5)
$\text{FeCl}_3$	26.3(9) : 73.7(9)	27(1) : 73(1)	23.5(6) : 76.5(6)	19(4) : 81(4)	38.5(8) : 61.5(8)	2.14(6)	87.4(9) : 12.6(9)
	1.6(2)	1.5(3)	1.90(9)	1.3(6)	0.78(7)		2.3(2)

Normalized product ratios are shown on top, while turnover numbers are shown at the bottom. All product ratios and turnover numbers were determined by GC analysis. All product ratios are normalized with respect to the number of 1°, 2°, and 3° C–H bonds. For reactions with  $\text{CCl}_4$ , turnovers are reported as moles product per mole  $\text{Fe}(\text{III})$ . For reactions without an external functional group donor, turnovers are reported as moles product per two moles of  $\text{Fe}(\text{III})$ . Values obtained as an average of three replicates are reported with the standard deviation enclosed in parenthesis.

aromatic ring situated close to the apical Fe–Cl bond (Figure 1 and Figure S1).  $[\mathbf{1}-(\text{CF}_3)_8][\text{B}(\text{C}_6\text{F}_5)_4]$  maintains selectivity against 3° C–H bonds despite displaying the highest activity and a turnover number exceeding one. These results suggest that the electron-withdrawing  $\text{CF}_3$  groups of  $[\mathbf{1}-(\text{CF}_3)_8]^+$  destabilize the  $\text{Cl}\cdot$ |arene complex to increase reactivity, while providing additional steric bulk to bolster selectivity (Figure S1).

The PDI complexes  $[\mathbf{1}][\text{B}(\text{C}_6\text{F}_5)_4]$ ,  $[\mathbf{1}][\text{FeCl}_4]$ ,  $[\mathbf{1}-(\text{CF}_3)_8][\text{B}(\text{C}_6\text{F}_5)_4]$ , and  $[\mathbf{1}-(\text{CF}_3)_8][\text{FeCl}_4]$  maintain enhanced C–H activation selectivity over  $\text{FeCl}_3$  in the photochlorination of a range of substrates (Table 2 and Tables S7–S13). Site specificity for chlorination of the 1° C–H bonds in 2,3-dimethylbutane (**3**) increases from 26% for  $\text{FeCl}_3$  to 97% for  $[\mathbf{1}][\text{B}(\text{C}_6\text{F}_5)_4]$ , highlighting the steric preference of these complexes for more accessible C–H bonds. The PDI complexes also shift reactivity towards 1° C–H bond functionalization compared to  $\text{FeCl}_3$  in the photochlorination of *n*-hexane (**4**) and 2,2-dimethylbutane (**5**). The steric bulk of the phenyl ring in ethylbenzene (**6**) results in a more pronounced increase in 1° selectivity (up to 90%) despite the presence of weak 2° benzylic C–H bonds. Adamantane (**7**) features a constrained ring structure with 3° C–H bonds that are more exposed than its 2° C–H bonds.<sup>36</sup> As a result, the PDI complexes display a greater preference for the activation of the 3° sites over the 2° sites of **7**. In general,  $[\mathbf{1}-(\text{CF}_3)_8]^+$  exhibited selectivities similar to  $[\mathbf{1}]^+$ , but with slightly higher activities (Tables S7–S13). For example,  $[\mathbf{1}-(\text{CF}_3)_8][\text{B}(\text{C}_6\text{F}_5)_4]$  showed over twice the activity of  $[\mathbf{1}][\text{B}(\text{C}_6\text{F}_5)_4]$  in the photochlorination of cyclohexane (**8**) to chlorocyclohexane (Table S11). Reactions with cyclohexene (**9**) yielded *trans*-1,2-dichlorocyclohexane in addition to chlorocyclohexene. The PDI

complexes favor chlorine addition to the cyclohexene double bond over C–H activation. This reactivity has been reported for  $\text{Cl}\cdot$  adducts with  $\text{Cl}^-$  and alcohols,<sup>26</sup> corroborating that photochlorination using the PDI complexes proceeds through the formation of a  $\text{Cl}\cdot$ |arene adduct. In contrast, reactions with  $\text{FeCl}_3$ , which can only generate  $\text{Cl}\cdot$ , were more selective for C–H chlorination.

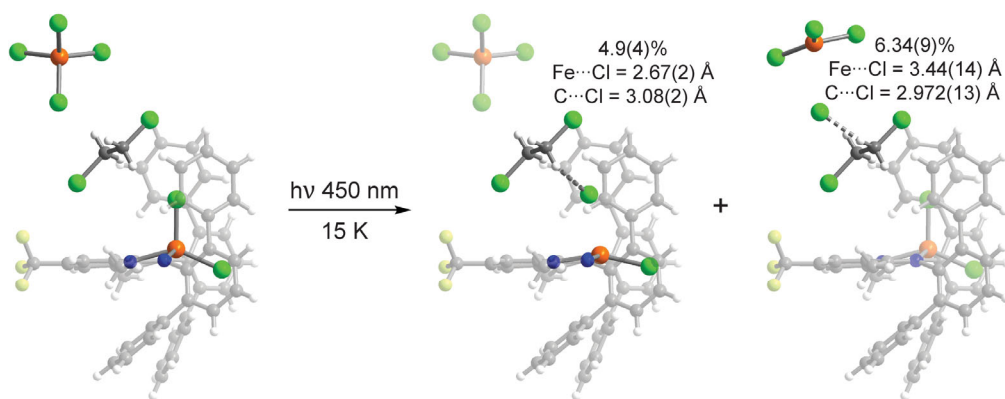
To expand the scope of selective C–H functionalization reactions,  $\text{CCl}_4$  was replaced with  $\text{BrCCl}_3$  (20 equiv) as a radical trap. Notably, reactions with the  $[\text{Fe}(\text{PDI})\text{Cl}_2][\text{B}(\text{C}_6\text{F}_5)_4]$  salts favored C–H bromination over chlorination with selectivity for more accessible C–H bonds (Entry 1, Table 3 and Table S6), whereas control experiments with  $\text{FeCl}_3$  and  $[(\text{Ph}_3\text{P})_2\text{N}][\text{FeCl}_4]$  yielded considerable amounts of chlorinated products (Entries 2 and 3, respectively, Table 3 and Table S6). These results demonstrate that the PDI complexes participate primarily in C–H activation of the substrate and allow for independent functionalization of the resulting carbon-centered radical by different functional group donors such as  $\text{BrCCl}_3$ .

**Photocrystallography Experiments.** Photocrystallographic experiments provides structural insight into the mechanism of C–H activation and confirmed that photolysis leads to activation of the apical Fe–Cl bond. X-ray diffraction data were collected as a single crystal of  $[\mathbf{1}][\text{FeCl}_4]\cdot(\text{DCE})$  ( $\text{DCE} = 1,2$ -dichloroethane; space group *Pbca*) was exposed to 450 nm light at 15 K. The structure obtained after 83 min irradiation reveals that both  $[\mathbf{1}]^+$  and  $[\text{FeCl}_4]^-$  undergo chlorine photoelimination (Figure 4 and Figure S6). Specifically, the apical  $\text{Fe}\cdots\text{Cl}$  distance of  $[\mathbf{1}]^+$  increases from 2.1520(3) to 2.67(2) Å, while the  $\text{Fe}\cdots\text{Cl}$  distance of one of the chloride ligands of  $[\text{FeCl}_4]^-$  lengthens from 2.1851(4) to 3.44(13) Å. These large  $\text{Fe}\cdots\text{Cl}$  separations exceed the sum of the ionic radius of high-spin

**Table 3.** Photobromination of 3-methylpentane using the  $[\mathbf{1}][\text{B}(\text{C}_6\text{F}_5)_4]$ ,  $\text{FeCl}_3$ , and  $[(\text{Ph}_3\text{P})_2\text{N}][\text{FeCl}_4]$  with  $\text{BrCCl}_3$  as Br atom donor.

Entry	Fe complex	R–Br : R–Cl product ratio	Normalized 1° : 2° : 3° product ratio <sup>a</sup>	Turnover <sup>b</sup>
1	$[\mathbf{1}][\text{B}(\text{C}_6\text{F}_5)_4]$	96.4(7) : 3.6(7)	33(2) : 57.1(3) : 10(2)	0.9(2)
2	$\text{FeCl}_3$	51(2) : 49(2)	19(4) : 12(2) : 69(7)	0.51(6)
3	$[(\text{Ph}_3\text{P})_2\text{N}][\text{FeCl}_4]$	81(1) : 19(1)	17.3(6) : 28.1(3) : 54.6(6)	1.3(2)

All product ratios and turnover numbers were determined by GC analysis. <sup>a</sup>Product ratios are normalized with respect to the number of 1°, 2°, and 3° C–H bonds. <sup>b</sup>Turnover numbers are reported as moles product per mole  $\text{Fe}(\text{III})$ . Values obtained as an average of three replicates are reported with the standard deviation enclosed in parenthesis.

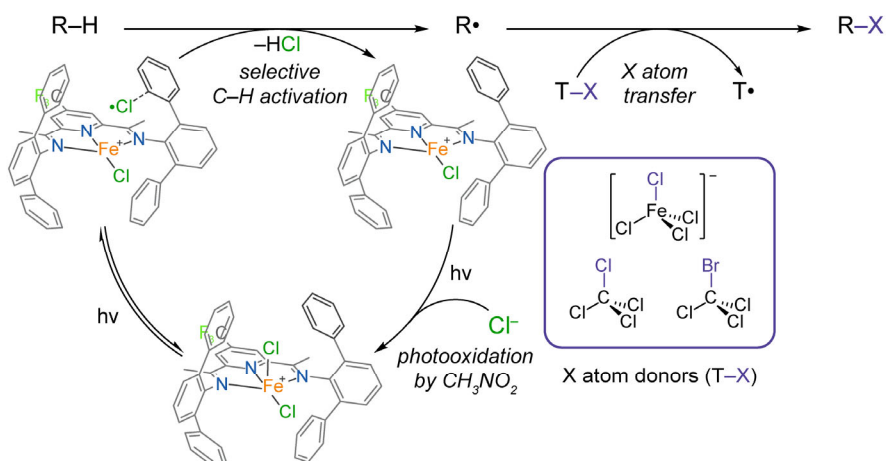


**Figure 4.** Photocrystallographic characterization of chlorine photoelimination in a single crystal of  $[1][FeCl_4] \cdot (DCE)$  (*Pbca*) as determined from X-ray diffraction data collected at 15 K. The Cl atoms of HCl molecules formed after C–H activation were located at sites close to the carbon atoms of DCE; the H atoms of these molecules were not located in the electron density difference map. Instead, dashed lines are drawn between the Cl atoms and the H atoms on DCE. Orange, green, light green, blue, gray, and white spheres represent Fe, Cl, F, N, C, and H atoms, respectively.

iron(II) and the van der Waals radius of Cl (2.53 Å),<sup>55</sup> consistent with photocleavage of the apical Fe–Cl bond of  $[1]^+$  and one of the Fe–Cl bonds of  $[FeCl_4]^-$ . The chlorine atom eliminated from  $[1]^+$  was located at relatively long distances ( $C \cdots Cl \geq 3.433(12)$  Å) away from the aromatic rings of PDI ligand, precluding assignment of the photoinduced structure as the  $Cl \cdot$  arene adduct. Instead, the chlorine atom engages in a close contact ( $C \cdots Cl = 3.08(2)$  Å) with the carbon atom of a nearby DCE solvent molecule. Similarly, the chlorine atom eliminated from  $[FeCl_4]^-$  also displays a close contact ( $C \cdots Cl = 2.972(13)$  Å) with one of the carbon atoms of the solvent molecule. These short  $C \cdots Cl$  distances, which are well within the sum of the van der Waals radii of C and Cl (3.45 Å), indicate that the photoeliminated chlorine radicals have activated the C–H bonds of DCE to yield HCl and carbon-centered radicals, which remain in contact through hydrogen bonding.<sup>42</sup> The photoinduced structures gradually increased in occupancy as the crystal was irradiated, reaching occupancies of 4.9(4)% and 6.34(9)% for the elimination products of  $[1]^+$  and  $[FeCl_4]^-$ , respectively (Figure S8). These results suggest that irreversible reaction between the photoeliminated chlorine radicals and DCE leads to accumulation of the photoproducts over the timescale of the experiment, which ultimately enables

observation of chlorine photoelimination. Accordingly, no photoinduced changes were observed for a polymorph of  $[1][FeCl_4] \cdot (DCE)$  (space group *P2<sub>1</sub>/c*) with no DCE solvent molecules proximal to the Fe–Cl bonds of  $[1]^+$  and  $[FeCl_4]^-$  (Figure S2). These photocrystallographic experiments further support that the iron(III) PDI complexes generate  $Cl \cdot$  within the steric environment defined by the iron secondary coordination sphere, which in turn imparts selectivity in chlorine radical-mediated C–H activation reactions.

Taking the spectroscopic, photochemical, and photocrystallographic experiments into account, Figure 5 shows the proposed mechanism for selective C–H functionalization. Irradiation of the iron(III) PDI complex results in cleavage of its apical Fe–Cl bond to give an iron(II) center and a chlorine radical. Upon elimination,  $Cl \cdot$  subsequently forms a charge-transfer complex with an aromatic ring in the iron secondary coordination sphere. The resulting adduct either rapidly recombines with the iron center or abstracts a hydrogen atom from a nearby substrate molecule. Although backreaction of  $Cl \cdot$  in the absence of substrate decreases the photochlorination quantum yields (Table S16), this process prevents escape of the radical from the iron coordination sphere and, as a result, ensures that the PDI complex controls the selectivity of chlorine-radical



**Figure 5.** Proposed mechanism for photocatalytic C–H activation by the  $[Fe(PDI)Cl_2]^+$  complexes followed by functionalization by different functional group donors.

mediated C–H bond activation. Selective activation of the substrate yields HCl and a hydrocarbon radical, which is ultimately functionalized by a radical trap such as  $[\text{FeCl}_4]^-$ ,  $\text{CCl}_4$ , or  $\text{BrCCl}_3$ . Photochemical oxidation of the iron(II) PDI complex by  $\text{CH}_3\text{NO}_2$ , along with addition of a chloride ligand, regenerates the initial iron(III) complex and closes the catalytic cycle.

## CONCLUSIONS

The foregoing results demonstrate that the secondary coordination sphere of a metal complex can enforce steric control over C–H activation by photoeliminated chlorine radicals. Specifically, a series of iron(III) chloride PDI complexes exhibit steric selectivity in photochemical C(sp<sup>3</sup>)–H chlorination and bromination reactions, favoring more accessible 1° and 2° C–H bonds over weaker 3° C–H bonds. Transient absorption spectroscopy confirms that these iron complexes stabilize photoeliminated  $\text{Cl}\cdot$  through formation of a  $\text{Cl}\cdot$ -arene complex with aromatic substituents on the PDI ligand. Moreover, photocrystallography experiments unveil that confinement of  $\text{Cl}\cdot$  within the iron secondary coordination sphere gives rise to the observed selectivity in chlorine-radical mediated C–H activation reactions.

Altogether, these results outline a secondary coordination sphere strategy to control the reactivity of chlorine radicals, which have long been regarded as potent yet unselective hydrogen-atom abstraction agents. This approach sets the stage for the integration of  $\text{Cl}\cdot$  and other highly reactive radical intermediates in catalyst- or reagent-controlled selective C–H functionalization reactions, expanding the scope of new and existing methodologies in organic photocatalysis.

## ASSOCIATED CONTENT

### Supporting Information

The Supporting Information is available free of charge on the ACS Publications website.

Materials and methods, synthetic schemes, details on the synthesis and characterization of the PDI ligand and iron(III) PDI complexes, additional crystallographic data, zero-field <sup>57</sup>Fe Mössbauer spectroscopy data, cyclic voltammetry data, additional photohalogenation results, and supplementary text for control experiments and TA spectroscopy, are available in the supplementary information.

### Accession Codes

Metrical data for the solid-state structures are available from the Cambridge Crystallographic Data Centre under reference numbers CCDC 2100012–2100021 contain the supplementary crystallographic data for this paper. These data can be obtained free of charge via [www.ccdc.cam.ac.uk/data\\_request/cif](http://www.ccdc.cam.ac.uk/data_request/cif), or by emailing [data\\_request@ccdc.cam.ac.uk](mailto:data_request@ccdc.cam.ac.uk), or by contacting The Cambridge Crystallographic Data Centre, 12 Union Road, Cambridge CB2 1EZ, UK; fax: +44 1223 336033.

## REFERENCES

- (1) Labinger, J. A.; Bercaw, J. E. Understanding and exploiting C–H bond activation. *Nature* **2002**, *417*, 507–514.
- (2) Arndtsen, B. A.; Bergman, R. G.; Mobley, T. A.; Peterson, T. H. Selective intermolecular carbon-hydrogen bond activation by synthetic metal complexes in homogeneous solution. *Acc. Chem. Res.* **1995**, *28*, 154–162.
- (3) Cernak, T.; Dykstra, K. D.; Tyagarajan, S.; Vachal, P.; Krska, S. W. The medicinal chemist's toolbox for late-stage functionalization of drug-like molecules. *Chem. Soc. Rev.* **2016**, *45*, 546–576.
- (4) Goldberg, K. I.; Goldman, A. S. Large-scale selective functionalization

## AUTHOR INFORMATION

### Corresponding Author

**Daniel G. Nocera** – Department of Chemistry and Chemical Biology, Harvard University, 12 Oxford Street, Cambridge, MA 02138–2902, United States; [orcid.org/0000-0001-5055-320X](http://orcid.org/0000-0001-5055-320X); E-mail: [dnocera@fas.harvard.edu](mailto:dnocera@fas.harvard.edu).

### Authors

**Miguel I. Gonzalez** – Department of Chemistry and Chemical Biology, Harvard University, 12 Oxford Street, Cambridge, MA 02138–2902, United States; [orcid.org/0000-0003-4250-9035](http://orcid.org/0000-0003-4250-9035)

**David Gygi** – Department of Chemistry and Chemical Biology, Harvard University, 12 Oxford Street, Cambridge, MA 02138–2902, United States; [orcid.org/0000-0001-9070-4973](http://orcid.org/0000-0001-9070-4973)

**Yangzhong Qin** – Department of Chemistry and Chemical Biology, Harvard University, 12 Oxford Street, Cambridge, MA 02138–2902, United States; [orcid.org/0000-0002-2450-521X](http://orcid.org/0000-0002-2450-521X)

**Qilei Zhu** – Department of Chemistry and Chemical Biology, Harvard University, 12 Oxford Street, Cambridge, MA 02138–2902, United States; [orcid.org/0000-0003-2327-7283](http://orcid.org/0000-0003-2327-7283)

**Elizabeth J. Johnson** – Department of Chemistry and Chemical Biology, Harvard University, 12 Oxford Street, Cambridge, MA 02138–2902, United States; [orcid.org/0000-0001-5704-0562](http://orcid.org/0000-0001-5704-0562)

**Yu-Sheng Chen** – ChemMatCARS, The University of Chicago, Argonne, IL 60439, United States; [orcid.org/0000-0002-7646-7761](http://orcid.org/0000-0002-7646-7761)

### Funding Sources

This research was supported by the National Science Foundation (NSF) Division of Chemistry under the grant number CHE-1855531.

### Notes

The authors declare no competing financial interest.

## ACKNOWLEDGMENT

M.I.G. acknowledges the Arnold and Mabel Beckman Foundation for an Arnold O. Beckman Postdoctoral Fellowship. D.G. and E.J.J. acknowledge the NSF for Graduate Research Fellowships. NSF's ChemMatCARS Sector 15 is supported by the Divisions of Chemistry and Materials Research, National Science Foundation, under grant number CHE-1834750. Use of the Advanced Photon Source, an Office of Science User Facility operated for the U.S. Department of Energy (DOE) Office of Science by Argonne National Laboratory, was supported by the DOE under Contract No. DE-AC02-06CH11357. We thank Matthew J. Nava, Thomas P. Keane, Suyin Grass Wang, Tieyan Chang, Ying-Pin Chen, and Jennifer X. Wang for experimental assistance and helpful discussions.

of alkanes. *Acc. Chem. Res.* **2017**, *50*, 620–626.

(5) Lin, R.; Amrute, A. P.; Pérez-Ramírez, J. Halogen-mediated conversion of hydrocarbons to commodities. *Chem. Rev.* **2017**, *117*, 4182–4247.

(6) Gunay, A.; Theopold, K. H. C–H bond activations by metal oxo compounds. *Chem. Rev.* **2010**, *110*, 1060–1081.

(7) Lyons, T. W.; Sanford, M. S. Palladium-catalyzed ligand-directed C–H functionalization reactions. *Chem. Rev.* **2010**, *110*, 1147–1169.



- (8) He, J.; Wasa, M.; Chan, K. S. L.; Shao, Q.; Yu, J.-Q. Palladium-catalyzed transformations of alkyl C–H bonds. *Chem. Rev.* **2017**, *117*, 8754–8786.
- (9) White, M. C. Adding aliphatic C–H bond oxidations to synthesis. *Science* **2012**, *335*, 807–809.
- (10) White, M. C.; Zhao, J. Aliphatic C–H oxidations for late-stage functionalization. *J. Am. Chem. Soc.* **2018**, *140*, 13988–14009.
- (11) Liu, W.; Groves, J. T. Manganese catalyzed C–H halogenation. *Acc. Chem. Res.* **2015**, *48*, 1727–1735.
- (12) Holmberg-Douglas, N.; Nicewicz, D. A. Photoredox-catalyzed C–H functionalization reactions. *Chem. Rev.* [Online early access]. DOI: 10.1021/acs.chemrev.1c00311. Published Online: Sept. 29, 2021. <https://pubs.acs.org/doi/abs/10.1021/acs.chemrev.1c00311> (accessed Oct. 5, 2021).
- (13) McBee, E. T.; Hass, H. B.; Neher, C. M.; Strickland, H. Chlorination of methane. *Ind. Eng. Chem.* **1942**, *34*, 296–300.
- (14) Hass, H. B.; McBee, E. T.; Weber, P. Chlorination of paraffins. *Ind. Eng. Chem.* **1936**, *28*, 333–339.
- (15) Kariofillis, S. K.; Doyle, A. G. Synthetic and Mechanistic implications of chlorine photoelimination in nickel/photoredox C(sp<sup>3</sup>)–H cross-coupling. *Acc. Chem. Res.* **2021**, *54*, 988–1000.
- (16) Abderrazak, Y.; Bhattacharyya, A.; Reiser, O. Visible-light-induced homolysis of earth-abundant metal-substrate complexes: A complementary activation strategy in photoredox catalysis. *Angew. Chem. Int. Ed.* **2021**, *60*, 21100–21115.
- (17) Treacy, S. M. Rovis, T. Copper catalyzed C(sp<sup>3</sup>)–H bond alkylation via photoinduced ligand-to-metal charge transfer. *J. Am. Chem. Soc.* **2021**, *143*, 2729–2735.
- (18) Kang, Y. C.; Treacy, S. M.; Rovis, T. Iron-catalyzed photoinduced LMCT: A 1° C–H abstraction enables skeletal rearrangements and C(sp<sup>3</sup>)–H alkylation. *ACS Catal.* **2021**, *11*, 7442–7449.
- (19) Rohe, S.; Morris, A. O.; McCallum, T.; Barriault, L. Hydrogen atom transfer reactions via photoredox catalyzed chlorine atom generation. *Angew. Chem. Int. Ed.* **2018**, *57*, 15664–15669.
- (20) Deng, H.-P.; Zhou, Q.; Wu, J. Microtubing-reactor-assisted aliphatic C–H functionalization with HCl as a hydrogen-atom-transfer catalyst precursor in conjunction with an organic photoredox catalyst. *Angew. Chem. Int. Ed.* **2018**, *57*, 12661–12665.
- (21) Deng, H.-P.; Fan, X.-Z.; Chen, Z.-H.; Xu, Q.-H.; Wu, J. Photoinduced nickel-catalyzed chemo- and regioselective hydroalkylation of internal alkynes with ether and amide  $\alpha$ -hetero C(sp<sup>3</sup>)H bonds. *J. Am. Chem. Soc.* **2017**, *139*, 13579–13584.
- (22) Shields, B. J.; Doyle, A. G. Direct C(sp<sup>3</sup>)–H cross coupling enabled by catalytic generation of chlorine radicals. *J. Am. Chem. Soc.* **2016**, *138*, 12719–12722.
- (23) Zidan, M.; Morris, A. O.; McCallum, T.; Barriault, L. The alkylation and reduction of heteroarenes with alcohols using photoredox catalyzed hydrogen atom transfer via chlorine atom generation. *Eur. J. Org. Chem.* **2020**, *10*, 1453–1458.
- (24) Nielsen, M. K.; Shields, B. J.; Liu, J.; Williams, M. J.; Zacuto, M. J.; Doyle, A. G. Mild, Redox-neutral formylation of aryl chlorides through the photocatalytic generation of chlorine radicals. *Angew. Chem. Int. Ed.* **2017**, *56*, 7191–7194.
- (25) Ackerman, L. K. G.; Alvarado, J. I. M.; Doyle, A. G. Direct C–C bond formation from alkanes using Ni-photoredox catalysis. *J. Am. Chem. Soc.* **2018**, *140*, 14059–14063.
- (26) Yang, Q.; Wang, Y.-H. Qiao, Y.; Gau, M.; Carroll, P. J.; Walsh, P. J.; Schelter, E. J. Photocatalytic C–H activation and the subtle role of chlorine radical complexation in reactivity. *Science* **2021**, *372*, 847–852.
- (27) Hu, A.; Guo, J.-J.; Pan, H.; Zuo, Z. Selective functionalization of methane, ethane, and higher alkanes by cerium photocatalysis. *Science* **2018**, *361*, 668–672.
- (28) Liu, W.; Groves, J. T. Manganese porphyrins catalyze selective C–H bond halogenations. *J. Am. Chem. Soc.* **2010**, *132*, 12847–12849.
- (29) Liu, W.; Huang, X.; Cheng, M.-J.; Nielsen, R. J.; Goddard, W. A.; Groves, J. T. Oxidative aliphatic C–H fluorination with fluoride ion catalyzed by a manganese porphyrin. *Science* **2012**, *337*, 1322–1325.
- (30) Chen, M. S.; White, M. C. Combined effects on selectivity in Fe-catalyzed methylene oxidation. *Science* **2010**, *327*, 566–571.
- (31) Hartwig, J. F. Catalyst-controlled site-selective bond activation. *Acc. Chem. Res.* **2017**, *50*, 549–555.
- (32) McMillan, A. J.; Sienkowska, M.; Lorenzo, P. D.; Gransbury, G. K.; Chilton, N. F.; Salamone, M.; Ruffoni, A.; Bietti, M.; Leonori, D. Practical and selective sp<sup>3</sup> C–H Bond Chlorination via aminium radicals. *Angew. Chem. Int. Ed.* **2021**, *60*, 7132–7139.
- (33) Short, M. A.; Shehata, M. F.; Sanders, M. A.; Roizen, J. L. Sulfamides direct radical-mediated chlorination of aliphatic C–H bonds. *Chem. Sci.* **2019**, *11*, 217–223.
- (34) Bakhoda, A. (Gus), Jiang, Q.; Badiei, Y. M.; Bertke, J. A.; Cundari, T. R.; Warren, T. H. Copper-catalyzed C(sp<sup>3</sup>)–H amidation: sterically driven primary and secondary C–H site-selectivity. *Angew. Chem. Int. Ed.* **2019**, *58*, 3421–3425.
- (35) Carestia, A. M.; Ravelli, D.; Alexanian, E. J. Reagent-dictated site selectivity in intermolecular aliphatic C–H functionalizations using nitrogen-centered radicals. *Chem. Sci.* **2018**, *9*, 5360–5365.
- (36) Quinn, R. K.; Könst, Z. A.; Michalak, S. E.; Schmidt, Y.; Szklarski, A. R.; Flores, A. R.; Nam, S.; Horne, D. A.; Vanderwal, C. D.; Alexanian, E. J. Site-selective aliphatic C–H chlorination using N-chloroamides enables a synthesis of chlorolissoclimide. *J. Am. Chem. Soc.* **2016**, *138*, 696–702.
- (37) Tierney, M. M.; Crespi, S.; Ravelli, D.; Alexanian, E. J. Identifying amidyl radicals for intermolecular C–H functionalizations. *J. Org. Chem.* **2019**, *84*, 12983–12991.
- (38) Bunce, N. J.; Ingold, K. U.; Landers, J. P.; Luszyk, J. Scaiano, J. C. Kinetic study of the photochlorination of 2,3-dimethylbutane and other alkanes in solution in the presence of benzene. First measurements of the absolute rate constants for hydrogen abstraction by the “free” chlorine atom and the chlorine atom-benzene  $\pi$ -complex. Identification of these two species as the only hydrogen abstractors in these systems. *J. Am. Chem. Soc.* **1985**, *107*, 5464–5472.
- (39) Russell, G. A. Solvent effects in the reactions of free radicals and atoms. II. Effects of solvents on the position of attack of chlorine atoms upon 2,3-dimethylbutane, isobutane and 2-deuterio-2-methylpropane. *J. Am. Chem. Soc.* **1958**, *80*, 4987–4996.
- (40) Hwang, S. J.; Powers, D. C.; Maher, A. G.; Anderson, B. L.; Hadt, R. G.; Zheng, S.-L.; Chen, Y.-S.; Nocera, D. G. Trap-free halogen photoelimination from mononuclear Ni(III) complexes. *J. Am. Chem. Soc.* **2015**, *137*, 6472–6475.
- (41) Hwang, S. J.; Anderson, B. L.; Powers, D. C.; Maher, A. G.; Hadt, R. G.; Nocera, D. G. Halogen photoelimination from monomeric Nickel(III) complexes enabled by the secondary coordination sphere. *Organometallics* **2015**, *34*, 4766–4774.
- (42) Gygi, D.; Gonzalez, M. I.; Hwang, S. J.; Xia, K. T.; Qin, Y.; Johnson, E. J.; Gygi, F.; Chen, Y.-S.; Nocera, D. G. Capturing the complete reaction profile of a C–H bond activation. *J. Am. Chem. Soc.* **2021**, *143*, 6060–6064.
- (43) Small, B. L. Discovery and development of pyridine-bis(imine) and related catalysts for olefin polymerization and oligomerization. *Acc. Chem. Res.* **2015**, *48*, 2599–2611.
- (44) Takaki, K.; Yamamoto, J.; Komeyama, K.; Kawabata, T.; Takehira, K. Photocatalytic oxidation of alkanes with dioxygen by visible light and copper(II) and iron(III) Chlorides: preference oxidation of alkanes over alcohols and ketones. *Bull. Chem. Soc. Jpn.* **2004**, *77*, 2251–2255.
- (45) Mereshchenko, A. S.; Olshin, P. K.; Karimov, A. M.; Yu. M.; Skripkin, Burkov, K. A.; Tveryanovich, Y. S.; Tarnovsky, A. N. Photochemistry of copper(II) chlorocomplexes in acetonitrile: trapping the ligand-to-metal charge transfer excited state relaxations pathways. *Chem. Phys. Lett.* **2014**, *615*, 105–110.
- (46) Hendrickson, D. N.; Kinnaird, M. G.; Suslick, K. S. Photochemistry of (5,10,15,20-tetraphenylporphyrinato)iron(III) halide complexes, Fe(TPP)(X). *J. Am. Chem. Soc.* **1987**, *109*, 1243–1244.
- (47) Kochi, J. K. Photolyses of metal compounds: cupric chloride in organic media. *J. Am. Chem. Soc.* **1962**, *84*, 2121–2127.



- (48) Nadtochenko, V. A.; Kiwi, J. Photolysis of  $\text{FeOH}^{2+}$  and  $\text{FeCl}^{2+}$  in aqueous solution. photodissociation kinetics and quantum yields. *Inorg. Chem.* **1998**, *37*, 5233–5238.
- (49) David, F.; David, P. G. Photoredox chemistry of iron(III) chloride and iron(III) perchlorate in aqueous media. A comparative study. *J. Phys. Chem.* **1976**, *80*, 579–583.
- (50) Fayad, R.; Engl, S.; Danilov, E. O.; Hauke, C. E.; Reiser, O.; Castellano, F. N. Direct evidence of visible light-induced homolysis in chlorobis(2,9-dimethyl-1,10-phenanthroline)copper(II). *J. Phys. Chem. Lett.* **2020**, *11*, 5345–5349.
- (51) Troian-Gautier, L.; Turlington, M. D.; Wehlin, S. A. M.; Maurer, A. B.; Brady, M. D.; Swords, W. B.; Meyer, G. J. Halide photoredox chemistry. *Chem. Rev.* **2018**, *119*, 4628–4683.
- (52) V. Yadav, R. J. Rodriguez, M. A. Siegler, D. P. Goldberg, Determining the inherent selectivity for carbon radical hydroxylation versus halogenation with  $\text{Fe}^{\text{III}}(\text{OH})(\text{X})$  complexes: Relevance to the rebound step in non-heme iron halogenases. *J. Am. Chem. Soc.* **2020**, *142*, 7259–7264.
- (53) *Fundamentals and Applications of Organic Electrochemistry: Synthesis, Materials, Devices*. 1st Ed.; Fuchigami, T., Atobe, M., Inagi, S., Eds; John Wiley & Sons: New York, **2015**.
- (54) Hudgens, J. W.; Johnson III, R. D.; Timonen, R. S.; Seetula, J. A.; Gutman, D. Kinetics of the reaction trichloromethyl + bromine and thermochemistry of trichloromethyl radical and cation. *J. Phys. Chem.* **1991**, *95*, 4400–4405.
- (55) Shannon, R. D. Revised effective ionic radii and systematic studies of interatomic distances in halides and chalcogenides. *Acta. Cryst.* **1976**, *A32*, 751–767.

---

TOC

